







## Article

# Structural Optimization and Experimental Validation of a Composite Engine Mount Designed for VTOL UAV

Milica Milić<sup>1,\*</sup> , Jelena Svorcan<sup>1</sup> , Toni Ivanov<sup>1</sup> , Ivana Atanasovska<sup>2</sup> , Dejan Momčilović<sup>3</sup> , Željko Flajs<sup>4</sup> and Boško Rašuo<sup>1</sup> 

<sup>1</sup> Faculty of Mechanical Engineering, University of Belgrade, 11000 Belgrade, Serbia; jsvorcan@mas.bg.ac.rs (J.S.); tivanov@mas.bg.ac.rs (T.I.); brasuo@mas.bg.ac.rs (B.R.)

<sup>2</sup> Mathematical Institute of the Serbian Academy of Sciences and Arts, 11000 Belgrade, Serbia; iatanasovska@mi.sanu.ac.rs

<sup>3</sup> Innovation Center of Faculty of Mechanical Engineering, University of Belgrade, 11000 Belgrade, Serbia; dbmomcilovic@mas.bg.ac.rs

<sup>4</sup> Institute for Testing of Materials IMS, 11040 Belgrade, Serbia; zeljko.flajs@institutims.rs

\* Correspondence: mmilic@mas.bg.ac.rs

**Abstract:** Unmanned air vehicles (UAVs) with vertical take-off and landing (VTOL) capabilities, equipped with rotors, have been gaining popularity in recent years for their numerous applications. Through joint efforts, engineers and researchers try to make these novel aircraft more maneuverable and reliable, but also lighter, more efficient and quieter. This paper presents the optimization of one of the vital aircraft parts, the composite engine mount, based on the genetic algorithm (GA) combined with the defined finite element (FE) parameterized model. The mount structure is assumed as a layered carbon composite whose lay-up sequence, defined by layer thicknesses and orientations, is being optimized with the goal of achieving its minimal mass with respect to different structural constraints (failure criteria or maximal strain). To achieve a sufficiently reliable structure, a worst-case scenario, representing a sudden impact, is assumed by introducing forces at one end, while the mount is structurally constrained at the places where it is connected to wings. The defined optimization methodology significantly facilitated and accelerated the mount design process, after which it was manufactured and experimentally tested. Static forces representing the two thrust forces generated by the propellers connected to electric engines (at 100% throttle and the asymmetric case where one engine is at approximately 40% throttle and the other at 100%) and loads from the tail surfaces were introduced by weights, while the strain was measured at six different locations. Satisfactory comparison between numerical and experimental results is achieved, while slight inconsistencies can be attributed to manufacturing errors and idealizations of the FE model.

**Keywords:** UAV; VTOL; composite; FE; optimization; GA; experiment



Academic Editor: Yaolong Liu

Received: 28 December 2024

Revised: 5 February 2025

Accepted: 20 February 2025

Published: 24 February 2025

**Citation:** Milić, M.; Svorcan, J.; Ivanov, T.; Atanasovska, I.; Momčilović, D.; Flajs, Ž.; Rašuo, B. Structural Optimization and Experimental Validation of a Composite Engine Mount Designed for VTOL UAV. *Aerospace* **2025**, *12*, 178. <https://doi.org/10.3390/aerospace12030178>

**Copyright:** © 2025 by the authors. Licensee MDPI, Basel, Switzerland. This article is an open access article distributed under the terms and conditions of the Creative Commons Attribution (CC BY) license (<https://creativecommons.org/licenses/by/4.0/>).

## 1. Background

In the field of aviation, the initial phase of the development process always begins with aerodynamics and the definition of the so-called aerodynamic scheme [1], followed by the analysis of aeroelastic and structural phenomena [2,3]. Phenomenologically, this class of problems includes a wide range of standardized methods and approaches; however, the emergence of new materials has led to many unresolved structural challenges. The increased use of composite materials, which are replacing metal materials in aviation, and modern production processes have instigated new classes of problems [2–4]. Due

to anisotropy and irregular shapes, the assessment of the behavior and load capacity of thin-walled curved structures remains a challenge, especially under combined loading conditions (when all stress components are present). Equations become more complex and often enter the domain of nonlinear calculations. Such calculations, due to their complexity, require larger and more advanced computational resources. Because of their specificity in sizing and forming computational models, composite materials in the optimization process necessitate the development of customized algorithms tailored to specific problem classes [4,5], as well as the use of approximated linear models for failure evaluation (based on various failure criteria defining the conditions under which any damage may occur in the laminate). Unmanned aerial vehicles (UAVs) have seen an expansion in application and exploitation across various industries, both civil and military [5,6]. In the civil sector, they are primarily used for agriculture, infrastructure inspection, logistics, etc. Their classification depends on flight autonomy, range, maximum take-off weight, payload size, etc. The aforementioned considerations in the design process can also be applied to UAVs, whose development has been extensively pursued worldwide over the past decade. There is a wide variety of configurations, sizes, materials, purposes, and specific working conditions, each requiring an individual engineering approach during both the design and operational and maintenance phases. This largely implies the necessity for experience and engineering practice in this class of problems as there are still no clearly established methods, standards, or procedures for the optimal sizing of structures and selection of components and equipment for the contemporary UAV structures [7].

The motivation for the current optimization study stems from the occurrence of the failure of the initial engine mount of a multipurpose UAV due to an unexpected impact loading (described in more detail in [8]). Since such load cases are becoming common for unmanned composite aircraft, it is necessary to start considering them seriously, even in the initial phases of aircraft design. It is also crucial to start designing and employing somewhat unconventional structural elements, such as asymmetric customized composite laminates, since they may contribute to improved performance and reliability in a wider range of operating conditions.

## 2. Introduction

UAVs with vertical take-off and landing (VTOL) capabilities have been gaining increasing significance due to their versatility and numerous applications. Thanks to advancements in rotor technologies, electric motors, and composite materials, UAVs are employed in various fields, ranging from logistics and agriculture to military and rescue operations. Their use in urban environments necessitates further improvements, such as enhanced maneuverability, reduced noise, and increased efficiency [9]. One of the key challenges in the development of these aircraft is the optimization of their structures to make them lighter, more reliable, and adaptable to demanding operating conditions. In addition, it is crucial to enable savings in time and resources at all stages of the design process, especially in the early phases. A particularly significant component of VTOL UAVs is the engine mount, which must withstand high loads induced by propeller thrust and external impacts while maintaining minimal mass. Traditional design methods are increasingly being replaced by advanced optimization techniques that combine numerical analyses and modern algorithms [10].

There is an increasing number of various optimization studies in aerospace applications, and here just a few of the newest ones are mentioned [11]. Researchers investigated and developed (simulate and experimentally test) composite materials for military UAVs operating in extreme environments [12]. Other researchers focused on the design and optimization of primary structures of tilt-duct rotors. By developing a FE model and defining

adequate load conditions, the authors managed to reduce the wing mass by nearly 39%. Similarly, researchers in [13,14] investigated and optimized carbon/epoxy laminates to predict and maximize the flutter speed of composite structures using Machine Learning and a Fast Tree Regression algorithm, respectively. Lastly, the authors of [15,16] performed a multi-objective optimization study of ultra-stable spacecraft structures from the aspects of mass and fundamental frequency by developing a parameterized structural model and employing response surface methodology.

The aim of this research is to develop a methodology for the preliminary design of composite structures based on the consideration of maximum load conditions. This methodology is established by integrating a genetic algorithm and finite element method (FEM) analysis, as well as incorporating the Tsai–Wu failure criterion into the background analyses [17,18]. The optimized structure is first validated through specimen testing, while the complete composite engine mount and the methodology itself are also experimentally verified, which is a general approach related to engineering structures [19].

The previously performed fracture analysis for impact loading on the same element is presented in [8]. The fracture analysis provided experimentally validated mechanical properties of the engine mount, as well as the distribution of the maximum loading used in the optimization of this structure. The goal of the present optimization is to achieve the minimal mass of the mount while meeting strict structural constraints, such as failure criteria and maximum deformation. The proposed methodology includes a simulation of the worst-case operational scenario, where the mount is subjected to sudden loads fully constrained at the attachment points to the wings. After optimization, the mount was manufactured and subjected to experimental tests. Static loads, representing propeller thrust at different power levels, were simulated using weights, while deformation was measured at multiple points along the structure. The obtained results demonstrate a high correlation between numerical and experimental data, with minor discrepancies attributed to manufacturing errors and FE model simplifications. This optimization approach accelerates the design process and enhances the performance of UAVs, paving the way for further development and application.

### 3. Methodology

#### 3.1. Optimization by the Genetic Algorithm

In the previous research [8], it was determined that the composite mount needs to be redesigned both geometrically and structurally after considering the complex load cases. To accomplish a structure of satisfactory reliability, that will remain operational in different working conditions, it is crucial to define an optimal arrangement of the laminate layers and increase overall resistance to similar impact/complex loads. The goal of the performed optimization is to minimize the mount mass (and other structural parameters) by determining the optimal arrangement of the laminate layers, as well as the necessary geometric changes, without compromising the existing mass-inertial model of the beam. The input parameters for this optimization are: six different thicknesses, six different orientations, and two hole sizes. In fact, the genetic algorithm (chosen for its fast convergence and wide applicability in numerous technical problems) integrated with the FEM analysis software (ANSYS Academic Research Mechanical 2019R3) should determine the best combination of input variables that define a structure capable to withstand the imposed constraints such as maximum stresses or the Tsai–Wu failure criteria [20,21]. In such cases, it is of great importance that the laminate has better impact energy absorption and resistance to impact loads, even though the load can be approximated as static. After evaluating various possibilities, two cases of the objective function were tested to address the presented optimization problem. The first case employs the weighted coefficient

method, ensuring that each term of the function is approximately equal to 1 and holds equal importance. This formulation considers all outputs simultaneously. The second case involves an objective function designed solely to minimize mass. These two approaches were tested to determine the optimal combination of parameters for achieving the best optimization accuracy.

Input parameters from FE analysis for the first objective function:

$$\begin{aligned} \text{mass [kg]} &= A_{1,1} \times 10^6, \\ \text{displacement [mm]} &= A_{2,1}, \\ \text{stress [MPa]} &= A_{3,1} \\ \text{strain} &= A_{4,1} \end{aligned} \quad (1)$$

The strain limit, expressed in terms of the carbon fiber properties and the safety factor ( $SF = 4$ , for long-term static load, strain boundary values, which are used in the failure analysis of the structure are provided in the literature [22]), has the following formulation:

$$\text{strain}_{limit} = \frac{0.0085}{SF} = \frac{0.0085}{4} \quad (2)$$

The mathematical formulation of the second objective function can be represented as dependence of  $f$  (minimal mass) with the constraint imposed by comparing the maximal computed strain relative to the strain limit. If  $\text{strain} < \text{strain}_{limit}$  the objective function considers only the mass:

$$f = \frac{\text{mass}}{1000} \quad (3)$$

If  $\text{strain} \geq \text{strain}_{limit}$ , the objective function is penalized with a large value:

$$f = 10^4 \quad (4)$$

This mathematical formulation reflects the logic in the MATLAB code and clearly expresses the relationships between the parameters in the objective function  $f$  and can be written in the following form:

$$f = \begin{cases} \frac{\text{mass}}{1000}, & \text{if } \text{strain} < \text{strain}_{limit} \\ 10^4, & \text{if } \text{strain} \geq \text{strain}_{limit} \end{cases} \quad (5)$$

The objective function  $f$  can be defined in a number of different ways, but is always calculated from the output parameters of the FE structural analysis that include total mass or laminate thickness, maximal displacement, stress, strain or failure coefficient, that are recorded in matrix A after every individual computation. This methodology allows flexible modeling in accordance with the desired final result, considering the imposed constraints. Along with the criteria used in this optimization algorithm, a basic evolutionary algorithm optimization with random search has been implemented. The goal is to minimize the objective function with constraints set according to the specified structural failure criteria. Figure 1 shows the optimization process flow for the selected objective function when minimizing mass.

The developed optimization algorithm with the described objective functions integrates two software packages, ANSYS Mechanical 2019R3 APDL and MATLAB2016. Within the operating function that is repeated for every considered individual, numerical calculations are performed based on variable input parameters, which define the parameterized geometric model, generate the finite element mesh, and apply the adequate boundary conditions. Then, a static analysis is executed in ANSYS Mechanical APDL, and values for mass, laminate thickness, displacement, stress, strain, and failure coefficient are saved

to file according to the given criteria. In MATLAB, the numbers of input parameters and boundaries for each variable of the design space are defined.

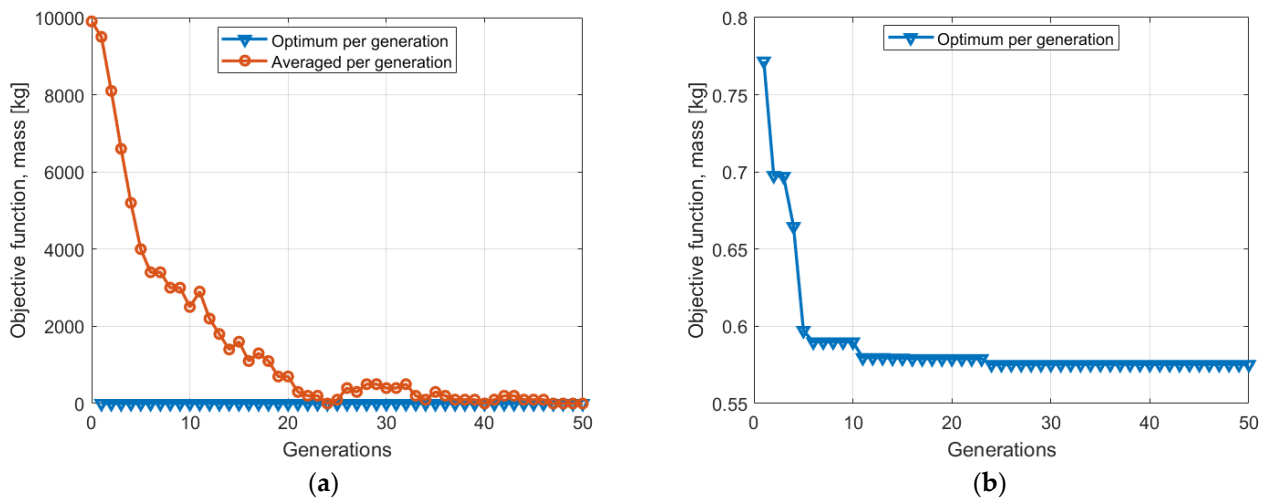


**Figure 1.** Optimization process when the objective function is minimal mass: (a) Averaging of the optimal solution: This involves evaluating multiple solutions and averaging the results to find a more robust and stable solution. In the case of mass, this could mean averaging the mass values obtained from several iterations or scenarios to minimize fluctuations and ensure a more reliable outcome. (b) Optimal solution in generation: This refers to finding the optimal solution during the generation of possible solutions. In this case, the optimal solution would be directly related to the mass value that meets the constraints and minimizes the objective function in the current generation of possible solutions. In both cases, the goal is to minimize or optimize the mass while considering the specific conditions and constraints of the problem.

Important for the calculation is the definition of the population size (`popSize`) and the maximum number of generations for each iteration (`maxGen`). For this problem, `popSize = 100` and `maxGen = 50` proved as being able to produce reliable and repeatable results/optimal solutions. Initialization of the variables, which store the best-found results, was performed with the `Inf` command, meaning that every valid solution found by the algorithm is considered better than the previous one. The main loop of the algorithm is initiated through a `for` loop that iterates through generations and each individual in the population. Only the first generation is formed randomly, while all subsequent generations are created through the processes of selection, crossover, and mutation, in accordance with the definition of the genetic algorithm. The output of this single-criterion process is a single optimized individual. A total of 14 input parameters, both structural and geometrical, were considered, while the output from every performed structural analysis comprises 6 parameters (previously mentioned). From these output parameters, different objective functions and constraints are further formed.

### 3.2. FE Model of the Mount

A parametric model of a shell mount was developed in ANSYS Mechanical APDL and is shown in Figure 2. Parametric modeling of complex geometries allows for quick modification of dimensions in later optimization stages. The beam has a circular cross-section with a diameter of 50 mm and a total length of 1670 mm. The weakened cross-section is located at two places on the beam, with a distance of 1300 mm between the centers of the cross-sections, which is also the distance between the motor axes. The openings at the weakened sections are through-holes for motor mounting. On the bottom side of the beam, the holes have a diameter of 6 mm, while the holes on the top side have a diameter of 2 mm and are threaded. The weight of the beam without the motor, with the vertical tail and

half of the horizontal tail, is 3790 g, while the weight of only the part of the beam being considered is 690 g.

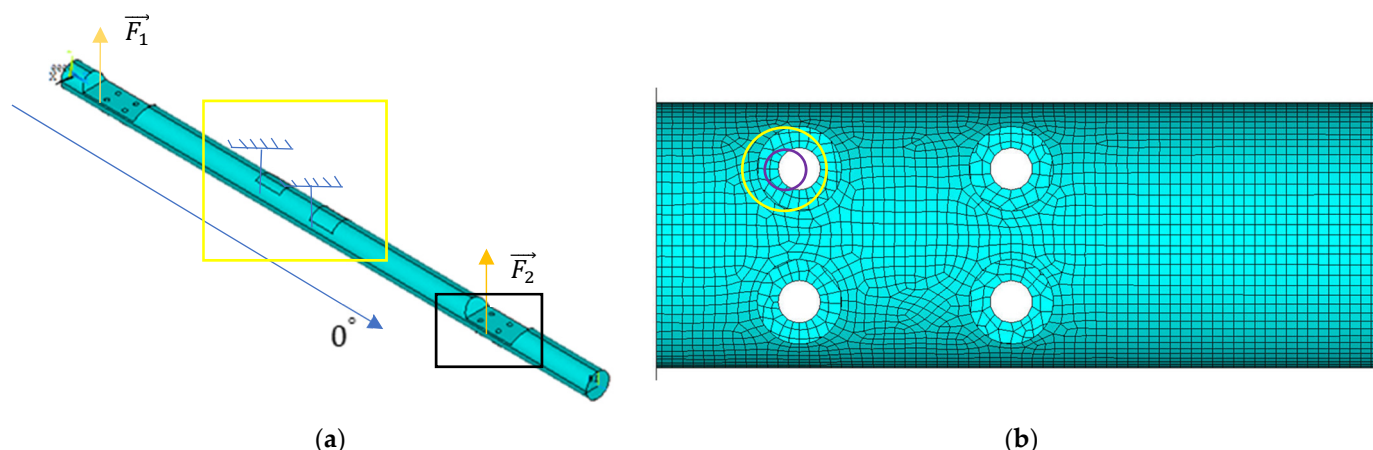


**Figure 2.** (a) The developed parametric engine mount model with boundary conditions, black rectangle indicates segment in b, blue arrows indicate the main direction of the laminate, orange arrows indicate the direction of the forces  $F_1$  and  $F_2$  (engine thrust), and the yellow square marks the location of the wing-spar connection (fixed support) (b) Mesh segment with marked dimensions  $R_1$  and  $R_2$ .

The mount was discretized into quadrilateral 6-layer shell elements SHELL181 (the stacking sequence is provided in Table 1, where the main stacking direction of the layers is  $0^\circ$  relative to the longitudinal axis of the beam, as shown in Figure 2). To ensure that the discretized finite element model does not significantly affect the results, a mesh convergence study was conducted. Several different element sizes, ranging from 10 mm to 1 mm, were tested under the same loading conditions. After the mesh convergence study, an element size of approximately 4 mm was adopted, resulting in a model with 10,975 nodes and 21,452 finite elements. Mesh segment is shown in Figure 2b where the yellow circle indicates the diameter  $R_1$ , while the purple one indicates  $R_2$ .

**Table 1.** Layer stacking of the laminate structure of the engine mount before optimization.

Number of Layers	$\theta$ [ $^\circ$ ]	$t$ [mm]
1	45	0.28
2	-45	0.28
3	90	0.28
4	0	0.45
5	-45	0.28
6	45	0.28
		Total: 1.85

### 3.3. Optimization Problem Formulation and Achieved Optimal Solutions

The optimization performed for this type of problem aimed to determine the optimal layer thicknesses, orientations, and geometric parameters (hole diameters) of the composite beam structure, ensuring minimal weight while maintaining structural integrity under different loading conditions. The problem was formulated as follows:

$$f_{cost} = \min M(x) \quad (6)$$

where  $M(x)$  represents the total mass of the structure, which is a function of the design variables  $x$ .

The optimization problem involves 14 design variables, which define the composite layup and geometry: layer thickness  $t_i$ , layer orientations  $\theta_i$ , hole diameters  $R_i$ . In that case, the design variable vector is:

$$x = \{t_1, \theta_1, t_2, \theta_2, t_3, \theta_3, t_4, \theta_4, t_5, \theta_5, t_6, \theta_6, R_1, R_2\} \quad (7)$$

The constants that participate in the formation of the optimization loop are:

1. Maximum stress  $\sigma_{max}(x) \leq \sigma_{allowable}$ ,
2. Maximum strain  $\varepsilon_{max}(x) \leq \varepsilon_{allowable}$ ,
3. Maximum displacement  $u_{max}(x) \leq u_{allowable}$ ,
4. Failure criteria Tsai–Wu  $F_{fail}(x) \leq 1$ , and
5. Physical bounds: layer thickness limit ( $t_{min} \leq t_i \leq t_{max} \forall i \in \{1, 2, 3, 4, 5, 6\}$ ); layer orientation ( $\theta_i \in \{0^\circ, 90^\circ, \pm 90^\circ\}$ ); hole diameters ( $R_1 \leq R_1, R_2 \leq R_{max}$ ).

Optimization was conducted for three distinct cases of load application to ensure that the redesigned structure satisfies all defined criteria. The maximum force value obtained from fracture analysis [8] is  $F = 1450$  N. The consolidated results, presented in Table 2, illustrate the optimal layer orientations aligned with the principal directions of the beam  $[0^\circ/90^\circ]$ . This configuration corresponds to the longitudinal direction, where the applied load (approximated as a static equivalent of the impact force) predominantly induces pure bending along the mount's axis, which coincides with the primary fiber orientation. Given the complexity of the loading conditions, with force components acting at specific angles—attributable to the combined effects of the vertical and horizontal stabilizers—it is imperative to predict fiber orientations capable of maintaining structural integrity under torsional loads. Accordingly, optimization was extended to include two additional scenarios:

**Table 2.** Optimal solutions for the three considered load cases.

	Thickness of Each Layer $t$ [mm]		Layer Orientation $\theta$ [°]		Diameter of the Hole on the Top Side of the Beam for Engine Mounting $R_1$ [mm]	Diameter of the Hole on the Bottom Side of the Beam for Engine Mounting $R_2$ [mm]
Case 1	$t_1$	0.41	$\theta_1$ (°)	17.6	5.9	1.08
	$t_2$	0.064	$\theta_2$ (°)	0		
	$t_3$	0.28	$\theta_3$ (°)	74.93		
	$t_4$	0.53	$\theta_4$ (°)	−1.87		
	$t_5$	0.37	$\theta_5$ (°)	0		
	$t_6$	0.34	$\theta_6$ (°)	0		
Total:		1.994				
Case 2	$t_1$	0.36	$\theta_1$ (°)	83.89	4.17	1.06
	$t_2$	0.27	$\theta_2$ (°)	2.55		
	$t_3$	0.054	$\theta_3$ (°)	63.88		
	$t_4$	0.56	$\theta_4$ (°)	2.43		
	$t_5$	0.25	$\theta_5$ (°)	82.86		
	$t_6$	0.05	$\theta_6$ (°)	66.53		
Total:		1.544				
Case 3	$t_1$	0.12	$\theta_1$ (°)	4.08	1.34	0.20
	$t_2$	0.06	$\theta_2$ (°)	25.81		
	$t_3$	0.29	$\theta_3$ (°)	57.02		
	$t_4$	0.56	$\theta_4$ (°)	−10.41		
	$t_5$	0.13	$\theta_5$ (°)	0		
	$t_6$	0.12	$\theta_6$ (°)	1.34		
Total:		1.28				

Case 1: Longitudinal loading, where the force induces bending along the primary fiber direction.

Case 2: Loading at a 60° angle, representing inertia effects from the vertical stabilizer and half of the horizontal stabilizer.

Case 3: Loading at a 45° angle, simulating dynamic conditions with combined directional force components.

The results for all three cases are integrated into Table 2, with annotations specifying the respective loading scenario for each optimal configuration. This approach ensures a comprehensive evaluation of the structural response under diverse loading conditions, providing a robust basis for the proposed design.

After conducting optimizations for several different combinations of the additional force component setup (which replaces the effect of the vertical and horizontal tails), the optimal layering of the new structure was selected and presented in Table 3. From the perspective of technologically feasible layer stacking, the orientations and thicknesses were chosen based on the optimized values, which are close to those values and material types that can be found in practical applications. The orientations were adjusted to values as close as possible to 0/90° and ±45°. A similarity was observed between the theoretically obtained values and those found in practical applications. The selected optimal stacking was determined empirically based on all the tested loads and taking into account the wet lay-up manufacturing process. In addition to the thickness and orientation of the layers, the holes on the top and bottom sides of the beam were optimized. The holes on the top side are for the motor's connection to the beam, while the holes on the bottom side were for mounting purposes.

**Table 3.** The selected optimal layering of the engine mount structure with parameters for the modified geometry.

	Thickness of Each Layer t [mm]		Layer Orientation $\theta$ [°]		Diameter of the Hole on the Top Side of the Beam for Engine Mounting $R_1$ [mm]	Diameter of the Hole on the Bottom Side of the Beam for Engine Mounting $R_2$ [mm]
Optimal Layering	$t_1$	0.23	$\theta_1$ (°)	45	4	0
	$t_2$	0.23	$\theta_2$ (°)	−45		
	$t_3$	0.23	$\theta_3$ (°)	90		
	$t_4$	0.56	$\theta_4$ (°)	0		
	$t_5$	0.23	$\theta_5$ (°)	−45		
	$t_6$	0.23	$\theta_6$ (°)	45		
	Total:	1.71				

The final optimized layering retains approximately the same mass-inertial model of the mount. The optimized mass of the beam is 554 g, which is approximately 19% lower than the initial, non-optimized structure. This difference is favorable from the perspective of aircraft operation, as it achieves a better mass-to-strength ratio. The diameter of the hole for the motor-beam connection remained unchanged at 4 mm, while the optimization resulted in a value of approximately 1 mm for the mounting holes. This value was set as the lower boundary in the objective function and actually represents the minimum, or 0 mm. The boundaries in the optimization algorithm for hole sizes were set so that all optimal values  $\leq 1$  indicate that the hole should not exist. This further suggests the disadvantage of having a weakened cross-section on the bottom side in cases of complex impact loads (due to the bending nature of the beam). The layer thicknesses indicate that the material type is carbon in epoxy resin, with a weave type of 160 g/m<sup>2</sup> for layers 1, 2, 3, 5, and 6, while layer 4 indicates a combination of two layers of 200 g/m<sup>2</sup> unidirectional carbon in epoxy resin.



## 4. Experimental Validation of the Optimized Laminate Structure

### 4.1. FEM Analysis of the Specimens with the Optimized Layering

In order to validate the optimization algorithm and test the selected optimal layering for the complex loading of the mount, standard laminate specimens were produced. All of them are rectangular with a length of 250 mm and a width of 25 mm, manufactured according to the standard [23]. The standard provides a procedure for testing the tensile properties of composite materials with a polymerized matrix. The parametric model of the specimen is shown in Figure 3a, while Figure 3b shows the detail of the finite element mesh of the specimen.

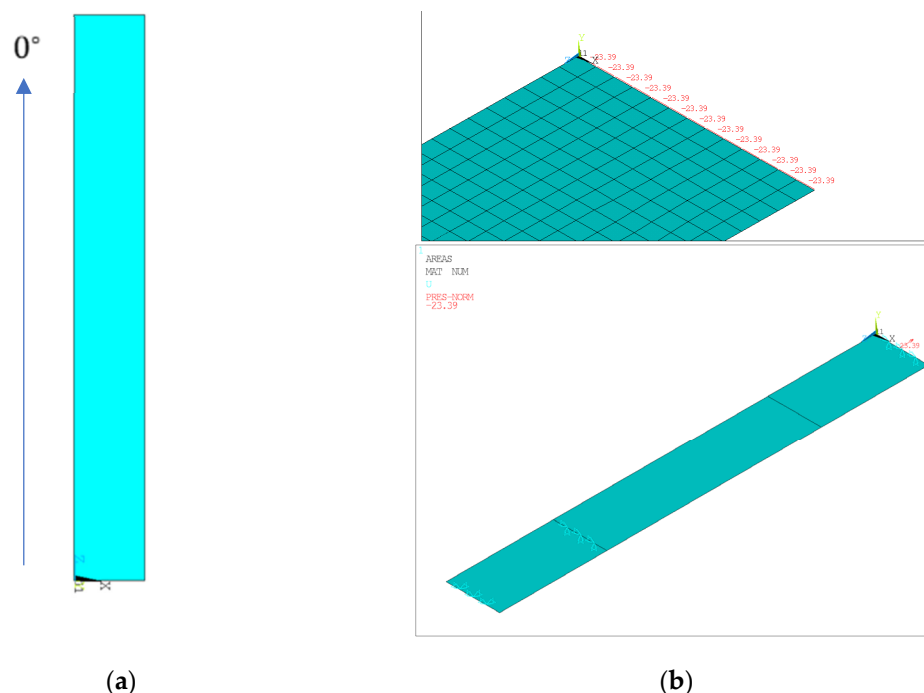


**Figure 3.** (a) Specimen model; (b) detail of the finite element mesh of the specimen.

Convergence of the results was achieved for square elements with an edge size of 1 mm. The total number of nodes is 5586, and the number of finite elements is 5293.

The material for forming the specimen model consists of the layer stacking obtained through optimization, as shown in Table 1. Considering that the results of the numerical analysis are compared with the results of experimental testing on a tensile testing machine, it is necessary to determine the maximum stress, displacement, and strain for the entire laminate. These values were determined based on defined failure criteria. The maximum stress criterion is a method used in material mechanics to find the highest stress value in the material and determine if the material has reached its endurance limit. This criterion takes into account the stress distribution in the material and how that distribution affects the occurrence of deformation. In this way, the Tsai–Wu failure criterion determines under which conditions the material will begin to deform. Additionally, the Tsai–Wu criterion defines the location of maximum stress in the material, which is important for predicting failure under loading conditions. The maximum stress in the specimen is 160.43 MPa, the maximum displacement is 0.475 mm, and the maximum strain is 0.4395%. A graphical representation of these results is shown in Figure 4, where (a) represents the maximum stress, (b) represents the maximum strain, and (c) represents the maximum displacement.

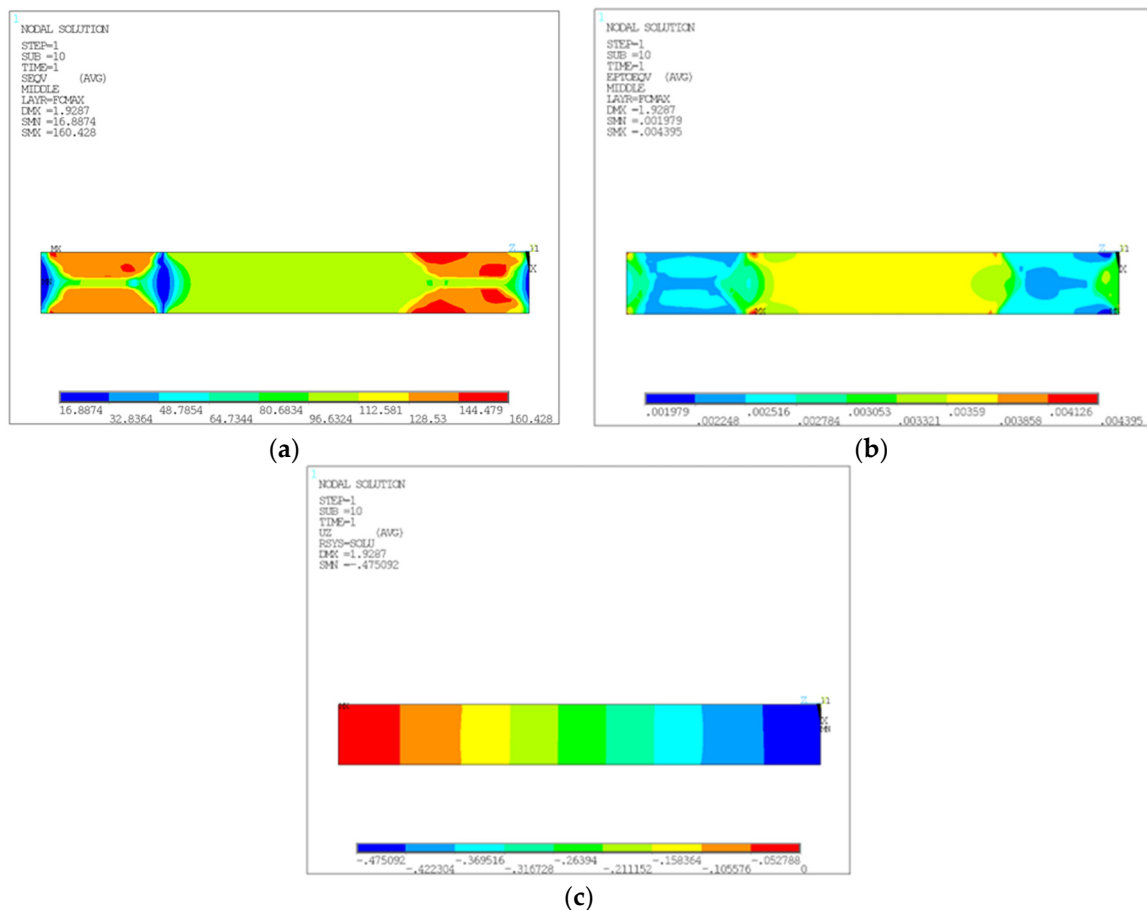


**Figure 4.** Numerical analysis of the specimen: (a) maximum stress, (b) maximum strain, and (c) maximum displacement.

#### 4.2. Experimental Analysis of the Specimens with the Optimized Layering

After conducting a detailed numerical analysis aimed at determining the optimal material characteristics and its behavior under various loading conditions, the sample preparation phase began. The goal was to reduce testing costs while ensuring high accuracy and reliability of the results. This was achieved through the manufacturing and testing of specimens.

This model allows for the consideration of various factors that can affect the material's behavior, such as layer orientation, thickness, and the properties of individual laminates. The samples were tested using the SHIMADZU AGX-V (SHIMADZU Cooperation, Kyoto, Japan) tensile testing machine. This machine was chosen due to its ability to provide high precision in measuring forces and instantaneous elongation during testing.

Sample preparation involved careful cutting and shaping to ensure that all samples had identical dimensions and shape. This is crucial for obtaining representative results, as any irregularity could affect the behavior of the sample during testing. Figure 5 shows all steps of sample preparation and their placement in the testing machine. This illustration helps in understanding the entire process and emphasizes the importance of careful preparation to obtain accurate and reliable test results.

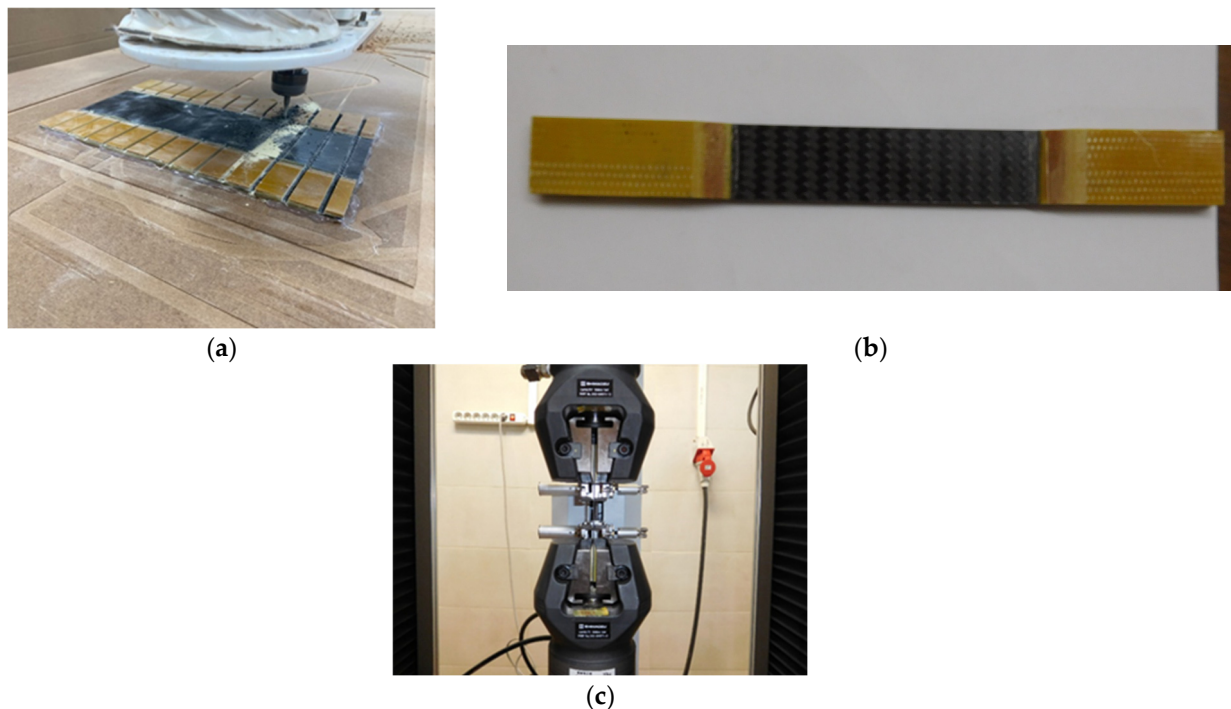


**Figure 5.** (a) Specimen fabrication, (b) appearance of the specimen for the new laminate stacking, and (c) experimental setup on the tensile testing machine.

#### 4.3. Experimental Analysis of the Optimized Mount

After validating the design and optimization procedure through comparison of numerical and experimental results for specimens, it was found that the optimized layering showed improved mechanical properties compared to the initial structure. This led to the construction of a new optimized engine mount, which included both structural and geometric changes, such as sealing the holes on the bottom of the mount. Due to equipment limitations, full-scale testing under maximum load was not possible. Instead, static testing was performed, representing the forces from the engine with tail effects. This experimental validation confirmed the established numerical model and methodology. The optimized mount exhibited better mechanical properties (complete absence of critical zones of concentrated stress, more adequate stress–strain trend, higher reliability measured by lower values of failure criteria), including lower mass, fulfilling safety requirements while using a new material type. The beam manufacturing used hand-lamination tools and vacuum processes. The presented experimental testing of the composite mount involves static loading, measured with strain gauges at selected locations for deflection in each individual loading case, both symmetric and asymmetric. The comparison of the results is focused on the deformations at the locations of the strain gauges and the relative error in relation to the numerical model. The testing was conducted with motor forces of 110 N and 130 N, applied parallel to the engine mounting points. Additionally, a constant mass of 3.1 kg was introduced, with a weight placed over a pulley to simulate the effect of half the weight of the horizontal tail. Figure 6 illustrates the designed experimental setup, with a yellow square marking the point of beam support and simulating the wing-beam connection, and a blue square marking the force application point. The testing used strain gauge instruments from the manufacturer TML (Alfred Amsler, Schaffhausen, Switzerland), labeled PLA 10-11, while data recording was performed using the modular HBM Quantum MX840B system (HBM, Darmstadt, Germany). This multipurpose modular system is used for precise measurement of various physical quantities. For data acquisition, the CatmanEasyAP software

(LabView) was used. To ensure the accuracy of the data, certified devices were used, and sensor/setup calibration was performed before the experiments.

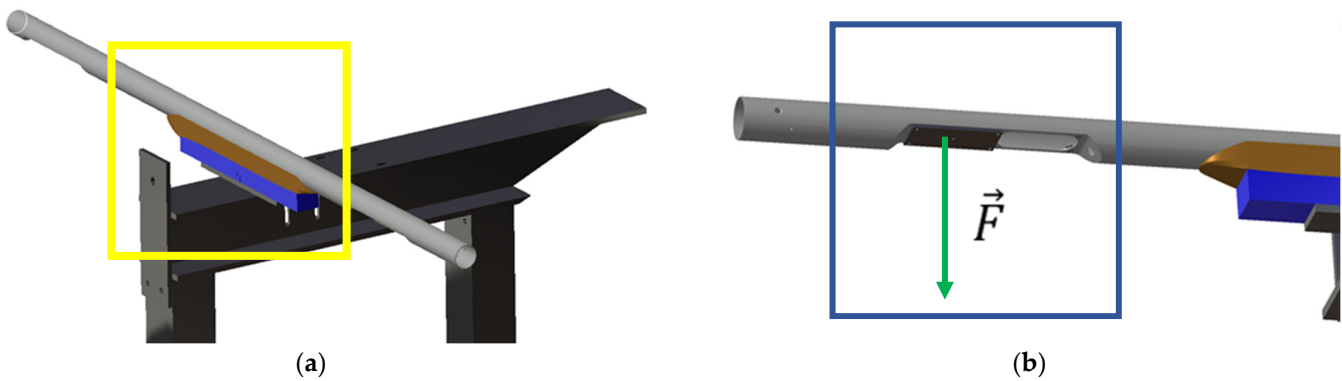


**Figure 6.** The designed experimental setup. (a) The yellow rectangle marks the location of the designed joint between the composite beam and the wing segment, while in image (b), the blue rectangle highlights the segment containing the electric motor, and the yellow arrow indicates the direction of the applied force  $F$ . The beam has been positioned in the opposite direction for testing purposes to simulate the actual force direction exerted by the motor.

The force on the tail in the experimental setup is applied through a pulley, while in the numerical model, it is approximated using an appropriate load transfer element to provide a more accurate numerical simulation (blue rectangular box). The specified boundary conditions, the wing–composite mount connection, are marked with a yellow rectangular box and represent a fixed joint. The mesh generation, selection of the finite element type, and material definition are identical to those described in detail in Section 3.2. According to the positions on the mount, measurement points are also defined in the numerical model to obtain the necessary values for comparative analysis. Figure 7 illustrates the experimental setup. In Figure 7a, the beam is subjected to static loading using weights, replicating the calculated thrust force of the engine, while Figure 7b presents the segment containing one of the measurement points.

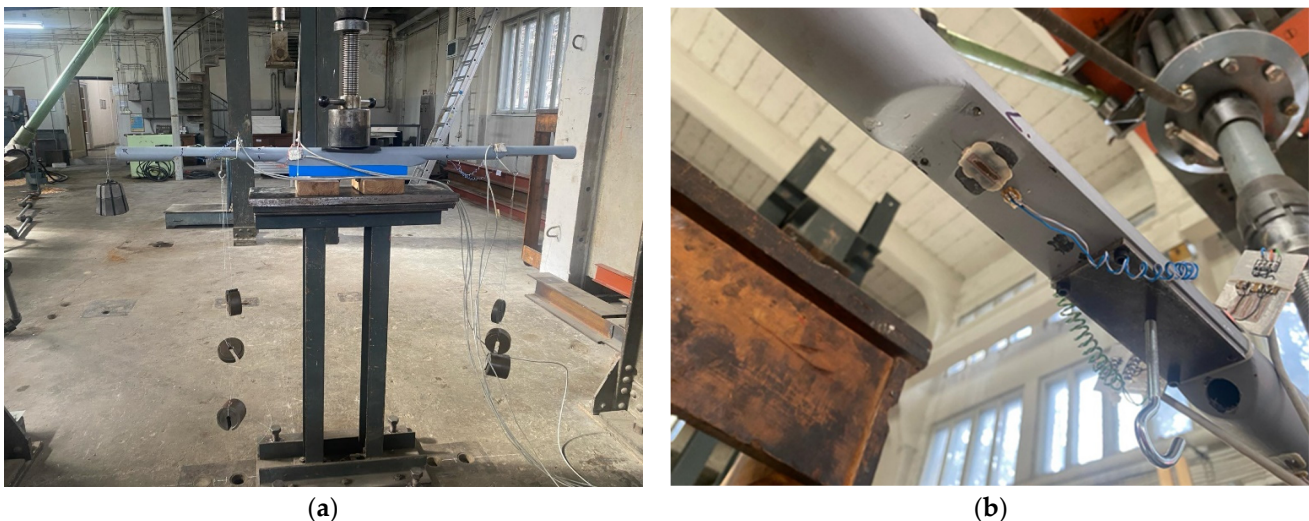


**Figure 7.** (a) The experimental setup of the engine mount; (b) measurement point.

## 5. Result and Discussion

### 5.1. Comparison of the Results of Numerical Analysis and Experimental Testing of the Specimens

In this section, a comparison of numerical and experimental results is presented to determine the validity of the applied numerical models and methods. The numerical models were developed using finite element analysis (FEA) software ANSYS Mechanical APDL, while the experimental results were obtained by testing samples on a SHIMADZU AGX-V tensile testing machine. The numerical results were obtained on the optimized parameterized model of the laminate specimen, simulating the tensile characteristics of the samples, including stresses and deformations under different loading conditions. The experimental samples were made with the same parameters as the numerical model and tested on the SHIMADZU AGX-V machine. Table 4 presents the comparative results of numerical and experimental analysis for key parameters: maximum stress, deformation at maximum stress, and Young's modulus. Based on the presented results, it can be observed that the numerical models show a high degree of agreement with the experimental data. The maximum stress calculated using the FEA model deviates by less than 13% compared to the experimentally obtained values, indicating relatively small error and high model precision. Similarly, the deformation at maximum stress and the Young's modulus show deviations of 17.8% and 6.25%, respectively, further confirming the reliability of the numerical analysis. The small deviations between the numerical and experimental results can be attributed to various factors, including idealization in the numerical model, variations in material properties, and the accuracy of experimental measurements. Despite these deviations, the numerical models provide a reliable foundation for predicting structural behavior under loading, enabling their application in further engineering analyses and optimizations. Based on these results, it can be concluded that the applied numerical models are valid and capable of representing real conditions with satisfactory accuracy. This comparison allows for additional verification and calibration of the models, achieving greater precision in future analyses and applied research.

**Table 4.** Comparative presentation of the results.

Specimen	E [GPa]	$\delta E$ [%]	$\sigma_{\max}$ [MPa]	$\delta \sigma_{\max}$ [%]	$\epsilon_{\max}$ [%]	$\delta \epsilon_{\max}$ [%]
Specimen 1	30.0	17.80	150	6.25	0.5	12.35
Specimen 2	32.5	10.95	130	18.75	0.4	10.11
Specimen 3	31.0	15.06	155	3.12	0.5	12.35
Specimen 4	30.0	17.80	150	6.25	0.5	12.35
Numerics	36.5	0.00	160	0.00	0.445	0.00

The appearance of failure on all the specimens after the application of the maximum load is shown on Figure 8, while stress–strain distributions for four selected specimens are illustrated in Figure 9.

The comparison of results presented in Table 4 is graphically shown in the form of diagrams in Figure 9a,b. The diagram in Figure 9a illustrates the relationship between stress and strain for the experimentally obtained values and the numerical values. Given the characteristics of the numerical model (where ideal bonding of laminate layers is assumed), the relationship between stress and strain is linear, whereas for the specimens, this characteristic slightly varies from sample to sample. These characteristics can also be observed in the diagram in Figure 9b, where the displacement in the numerical model is linear in relation to the increase in tensile force, indicating that the manufacturing technology significantly influences the mechanical characteristics of the laminate.



Figure 8. Tested specimens.

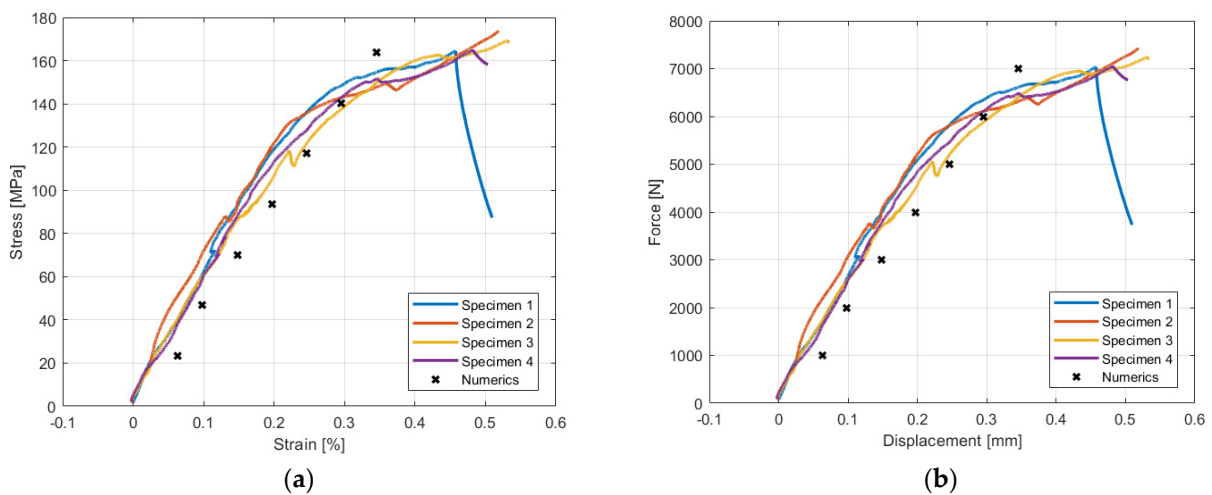


Figure 9. (a) Stress distribution on the specimen; (b) displacement distribution in the direction of deformation.

Based on the comparison of the stress–strain and force–displacement diagrams for the experimental samples and the numerical model, it can be concluded that there is a higher degree of agreement between the results. Experimental data obtained from the SHIMADZU AGX-V machine showed specific points of yielding and maximum stresses that are in good correlation with the numerical predictions obtained using the finite element method. The nature of this material is such that it has greater ductility compared to the previous layering combination (Table 1). These mechanical characteristics of the material are more favorable from the perspective of impact loading and the absorption of large kinetic energy that occurs during complex impact loading in a short time interval.

### 5.2. Comparison of the Results of Numerical Analysis and Experimental Testing of the Engine Mount

The first loading case of the composite engine mount involves an asymmetric load of 130 N on one engine and 50 N on the other engine, without neglecting the influence of the tail. These forces are equivalent to the load generated by both engines simultaneously during a flight condition with a changing aircraft position. The simulation of this loading case aims to replicate typical operating conditions when the engines are working at different throttle levels. The results obtained from the simulation and experimental tests are

presented in Table 5, with a graphical representation of the deformation behavior of the composite engine mount shown in Figure 10. These results are crucial for understanding how the mount responds under these operational conditions, providing insight into both deflection and strain distribution across the structure. In this case, despite the differences in the input load values, measurement points 1 and 5 exhibit approximately the same values, but with different directions of deformation. This is due to the introduction of a larger force closer to the tail, where the resultant force of the tail's weight and the force from the left engine are approximately equal to the force replacing the influence of the right engine.

**Table 5.** Loading case: left engine 13 kg + right engine 5 kg + tail.

	Experimental Values ( $\mu\text{m/m}$ )	Numerical Values ( $\mu\text{m/m}$ )
Measurement point 1	$-105.8838 \pm 10.00$	-51.3500
Measurement point 2	$27.4984 \pm 10.00$	31.5900
Measurement point 3	$-26.0652 \pm 10.00$	15.5500
Measurement point 4	$0.7820 \pm 10.00$	-11.1900
Measurement point 5	$105.8076 \pm 10.00$	77.5300
Measurement point 6	$-51.3814 \pm 10.00$	-62.8600

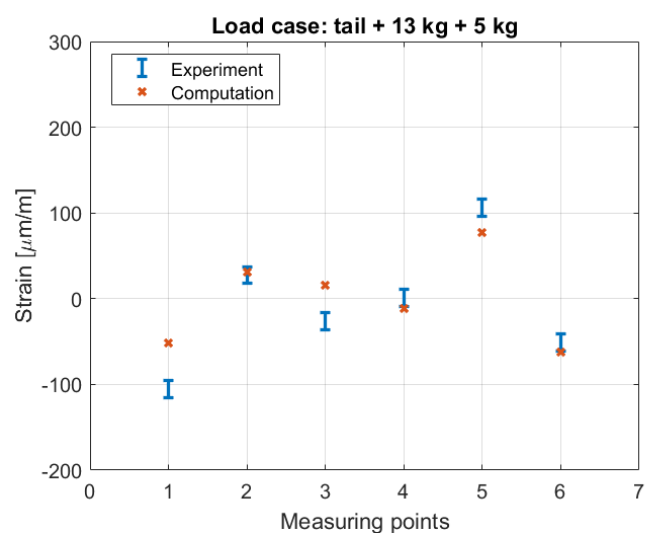


**Figure 10.** The graphical comparison of the results presented in Table 5.

The second loading case involves a symmetric simulation of two thrust forces of 130 N, applied in parallel at the positions of the left and right motors. This case also includes the influence of the tail, which adds complexity to the deformation pattern due to the additional weight distribution. The forces applied in this scenario correspond to a full throttle condition, which is a more extreme operational state compared to the first loading case. The comparison of experimental and numerical values for this loading case is presented in Table 6, and the corresponding graphical representation can be found in Figure 11.

The results reveal significant insights into the load distribution and deformation behavior. Notably, the values obtained at measurement points 1, 5, and 6, which are located at the furthest points of the mount, indicate that the influence of the tail weight is substantial. Despite the forces being symmetrically applied at the engine positions, the added mass of the tail introduces an asymmetry in the deformation, resulting in changes to the overall deflection pattern of the mount. This underscores the importance of considering not only the engine loads but also the contributions from other structural components, such

as the tail, when analyzing the performance of the composite engine mount under different operational conditions.

**Table 6.** Loading case: left engine 13 kg + right engine 13 kg + tail.

	Experimental Values ( $\mu\text{m/m}$ )	Numerical Values ( $\mu\text{m/m}$ )
Measurement point 1	$-108.1474 \pm 10.00$	-51.350
Measurement point 2	$28.3260 \pm 10.00$	31.5900
Measurement point 3	$-31.2116 \pm 10.00$	15.4900
Measurement point 4	$0.3396 \pm 10.00$	-11.3100
Measurement point 5	$283.0372 \pm 10.00$	205.8000
Measurement point 6	$-133.9242 \pm 10.00$	-162.200

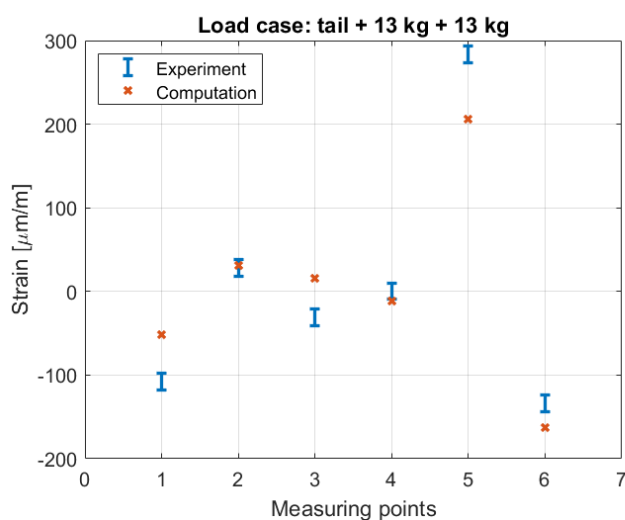


**Figure 11.** The graphical comparison of the results presented in Table 6.

The validation performed is based on measuring elastic deformations. The compared values, as can be seen in the diagrams, follow the same trend for each individual loading case and generally remain within the range of absolute measurement error. This indicates consistency in the direction of deviation, which may be the result of various factors, such as the sensitivity of measuring instruments to small deformations and the quality of the manufacturing of measuring devices. Additionally, the deviation between the numerical and experimental values can be attributed to the differences in the positions of the value readings provided by the strain gauges and the numerical node from which the numerical value was extracted. In addition the reading positions, the deformation of the strain gauge itself also influences the discrepancies in the values. Accordingly, the differences are considered acceptable.

### 6. Conclusions

The research presented in this paper outlines the methodology of the optimization process based on the calculated and predicted loads, which were considered in the early phases of the aircraft design. It can be concluded that, in addition to conventional analyses and verifications of components and elements of aerospace structures, additional review, calculations, and testing under real working conditions should be performed when structures contain locations with any kind of stress concentrators (geometric or material-related). The appearance of stress concentration can lead to delamination of the composite structure as well as failure in a specific element. One such element, the engine mount (composite



beam), which supports electric motors for vertical take-off and landing (VTOL) of the UAV, is discussed in this paper from the standpoint of optimization using an evolutionary optimization algorithm (the genetic algorithm). Detailed finite element method (FEM) calculations were performed and different input and output parameters for the optimization algorithm were defined. The optimization process, using the genetic algorithm, was carried out for 14 input variables (structural and geometric). The output from the structural analysis consists of 6 parameters (stress, mass, deformation, displacement, failure coefficient, and total laminate thickness). The result of the optimization is the geometric redesign of the engine mount's lower side, in the form of closing the motor mounting holes, as well as the optimal layering and orientation of the global laminate for approximated complex impact loading. The optimal layering was validated by testing composite specimens on a tensile testing machine. The mount model, whose structural and geometric modifications were obtained through optimization, was experimentally tested. The correspondence of the comparison between numerical and experimental results is at a satisfactory level, considering the mount's manufacturing technology and the impossibility of creating an ideal model as used in the numerical simulation. Additionally, the measurement results were influenced by the deformation of the strain gauge itself, as well as the sensitivity of the strain gauges and the measurement position relative to the numerical node position.

**Author Contributions:** Conceptualization, M.M. and J.S.; methodology, M.M.; software, M.M., J.S. and I.A.; validation, M.M., D.M. and Ž.F.; formal analysis, M.M., J.S., T.I. and I.A.; investigation, all authors; writing—original draft preparation, M.M.; writing—review and editing, M.M., J.S. and T.I.; visualization, M.M.; supervision, B.R. All authors have read and agreed to the published version of the manuscript.

**Funding:** This research was funded by the Ministry of science, technological development and innovation of Republic of Serbia by Contracts: 451-03-65/2024-03/200105, 451-03-66/2024-03/200029 and 451-03-66/2024-03/200213 from 5 February 2024.

**Data Availability Statement:** Dataset available on request from the authors.

**Conflicts of Interest:** The authors declare no conflict of interest.

## Abbreviations

The following abbreviations are used in this manuscript:

UAV	Unmanned arial vehicle
FEM	Finite element method
GA	Genetic algorithm
VTOL	Vertical take-off and landing
FEA	Finite element analysis

## References

1. Escobar-Ruiz, A.G.; Lopez-Botello, O.; Reyes-Osorio, L.; Zambrano-Robledo, P.; Amezcua Brooks, L.; Garcia-Salazar, O. Conceptual Design of an Unmanned Fixed-Wing Aerial Vehicle Based on Alternative Energy. *Int. J. Aerosp. Eng.* **2019**, *8104927*. [[CrossRef](#)]
2. Sheng, T.K.; Esakki, B.; Ponnambalam, A. Finite Element Analysis of Amphibian UAV Structure. In *Advances in Engineering Design and Simulation, Lecture Notes on Multidisciplinary Industrial Engineering*; Li, C., Chandrasekhar, U., Onwubolu, G., Eds.; Springer: Singapore, 2020. [[CrossRef](#)]
3. Grbović, A.; Kastratović, G.; Božić, Ž.; Božić, I.; Obradović, A.; Sedmak, A.; Sedmak, S. Experimental and numerical evaluation of fracture characteristics of composite material used in the aircraft engine cover manufacturing. *Eng. Fail. Anal.* **2022**, *137*, 106286. [[CrossRef](#)]
4. Skarka, W.; Jałowicki, A. Automation of a Thin-Layer Load-Bearing Structure Design on the Example of High Altitude Long Endurance Unmanned Aerial Vehicle (HALE UAV). *Appl. Sci.* **2021**, *11*, 2645. [[CrossRef](#)]

5. Zhennan, H. Analysis of After Impact Characteristics and Structural Optimization of CFRP Composite Plate. Master's Thesis, Embry-Riddle Aeronautical University, Daytona Beach, FL, USA, 2020.
6. Zimmermann, N.; Wang, P.H. A review of failure modes and fracture analysis of aircraft composite materials. *Eng. Fail. Anal.* **2020**, *115*, 104692. [[CrossRef](#)]
7. Torenbeek, E. *An Appreciation of Subsonic Engine Technology. Synthesis of Subsonic Airplane Design*; Springer: Dordrecht, The Netherlands, 1982; pp. 97–139. [[CrossRef](#)]
8. Milic, M.; Svorcan, J.; Zoric, N.; Atanasovska, I.; Momcilovic, D. Mathematical modeling and experimental investigation of a composite beam failure—Case study. *Proc. Inst. Mech. Eng. Part C J. Mech. Eng. Sci.* **2023**, *238*, 654–665. [[CrossRef](#)]
9. Mascarenhas, W.N.; Ahrens, C.H.; Ogliari, A. Design criteria and safety factors for plastic components design. *Mater. Des.* **2003**, *25*, 257–261. [[CrossRef](#)]
10. Wang, R.; Zhou, Z.; Ishibuchi, H.; Liao, T.; Zhang, T. Localized Weighted Sum Method for Many-Objective Optimization. *IEEE Trans. Evol. Comput.* **2018**, *22*, 3–18. [[CrossRef](#)]
11. Kim, B.-J.; Oh, C.-B.; Won, J.S.; Lee, H.I.; Lee, M.Y.; Kwon, S.H.; Lee, S.G.; Park, H.; Seong, D.G.; Jeong, J.; et al. Development of high-toughness aerospace composites through polyethersulfone composition optimization and mass production applicability evaluation. *Compos. Part A Appl. Sci. Manuf.* **2025**, *189*, 108590. [[CrossRef](#)]
12. Xu, S.; Liu, Y.; Zhang, J.; Zheng, Y. Preliminary Design and Optimization of Primary Structures for a Tilt-Duct UAV. *Aerospace* **2024**, *11*, 286. [[CrossRef](#)]
13. Dinulović, M.; Benign, A.; Rašuo, B. Composite Fins Subsonic Flutter Prediction Based on Machine Learning. *Aerospace* **2024**, *11*, 26. [[CrossRef](#)]
14. Li, X.; Qian, W.; Xiao, L.; Ai, X.; Liu, J. Optimized Design and Test of Geometrically Nonlinear Static Aeroelasticity Model for High-Speed High-Aspect-Ratio Wing. *Aerospace* **2024**, *11*, 1015. [[CrossRef](#)]
15. Dinulović, M.; Bengin, A.; Krstić, B.; Dodić, M.; Vorkapić, M. Flutter Optimization of Carbon/Epoxy Plates Based on a Fast Tree Algorithm. *Aerospace* **2024**, *11*, 636. [[CrossRef](#)]
16. Liu, C.; Xu, Z.; Han, K.; Han, C.; He, T. Optimization Design of Core Ultra-Stable Structure for Space Gravitational Wave Detection Satellite Based on Response Surface Methodology. *Aerospace* **2024**, *11*, 518. [[CrossRef](#)]
17. Roskam, J. *Airplane Design I-VIII*; Roskam Aviation and Engineering Corporation: Ottawa, ON, Canada, 1987.
18. Li, S.; Sitnikova, E.; Liang, Y.; Kaddour, A.-S. The Tsai-Wu failure criterion rationalised in the context of UD composites. *Compos. Part A Appl. Sci. Manuf.* **2017**, *102*, 207–217. [[CrossRef](#)]
19. Momčilović, D.; Odanović, Z.; Mitrović, R.; Atanasovska, I.; Vuherer, T. Failure analysis of hydraulic turbine shaft. *Eng. Fail. Anal.* **2012**, *20*, 54–66. [[CrossRef](#)]
20. Goldberg, D.E. *Genetic Algorithms in Search, Optimization, and Machine Learning*; Pearson Education, Inc.: Noida, India, 2005.
21. Le Riche, R.; Haftka, R.T. Improved genetic algorithm for minimum thickness composite laminate design. *Compos. Eng.* **1995**, *5*, 143–161. [[CrossRef](#)]
22. Kassa, M.K.; Singh, L.K.; Arumugam, A.B. Numerical and experimental investigation of first ply failure response of multi-walled carbon nanotubes/epoxy/glass fiber hybrid laminated tapered curved composite panels. *Proc. Inst. Mech. Eng. Part C J. Mech. Eng. Sci.* **2022**, *236*, 8481–8496. [[CrossRef](#)]
23. *ASTM D3039/D3039M-14*; Standard Test Method for Tensile Properties of Polymer Matrix Composite Materials, Section 7.1.2. ASTM International: West Conshohocken, PA, USA, 2014.

**Disclaimer/Publisher's Note:** The statements, opinions and data contained in all publications are solely those of the individual author(s) and contributor(s) and not of MDPI and/or the editor(s). MDPI and/or the editor(s) disclaim responsibility for any injury to people or property resulting from any ideas, methods, instructions or products referred to in the content.